

RESEARCH ARTICLE

A new impact model for the flexible rocking oscillator

Huanian Zhu  | Manolis N. Chatzis  | Sinan Acikgoz 

Department of Engineering Science, The University of Oxford, Oxford, UK

Correspondence

Huanian Zhu, Department of Engineering Science, The University of Oxford, Parks Road, Oxford OX1 3PJ, UK.
Email: huanian.zhu@eng.ox.ac.uk

Present address

Department of Engineering Science, The University of Oxford, Parks Road, Oxford OX1 3PJ, UK.

Abstract

Motivated by the rocking motion of non-rigid structures during earthquakes, this paper investigates the rocking behaviour of laterally flexible oscillators. Previous studies in this area utilised ad hoc assumptions to consider transitions between different motion phases at impact. Some models explored direct transitions between two rocking phases assuming that elastic translational velocities remain the same, while others assumed the dissipation of all vertical momentum after a rocking phase, leading to a full contact phase upon impact. In this paper, an improved impact model is proposed, where consistent mechanical principles are used to determine the phase transition criteria. The model departs from the principle that the spring and damper elements of the oscillator cannot transfer horizontal impulses over infinitesimally small durations. Alongside other mechanical constraints, this principle yields a series of momentum equations, which are solved to determine the post-impact velocities when transiting from one rocking phase to another. Through these equations, it is shown that a transition to full contact implies a specific locus of the vertical impulse from the support medium. Analytical and numerical investigations are then conducted to comparatively evaluate the new impact model. It is demonstrated that the new impact model yields equivalent results to established rigid rocking impact models for effectively rigid structures and resolves long-standing issues associated with excessive energy dissipation observed in previous models. Time histories of free rocking motion and stability analyses under pulse excitations are used to illustrate and generalise the findings for a range of geometries.

KEYWORDS

analytical model, impact, lateral flexibility, rocking

1 | INTRODUCTION

Rocking motion is typically encountered when bodies are connected through interfaces that do not offer tensile resistance. Utilising his pioneering rocking model (the inverted pendulum model or the IPM), Housner^[1] explained the surprisingly stable behaviour of tall and slender structures during earthquakes. An important assumption of the IPM is that the rocking structure is rigid.

This is an open access article under the terms of the [Creative Commons Attribution-NonCommercial-NoDerivs](https://creativecommons.org/licenses/by-nc-nd/4.0/) License, which permits use and distribution in any medium, provided the original work is properly cited, the use is non-commercial and no modifications or adaptations are made.

© 2022 The Authors. *Earthquake Engineering & Structural Dynamics* published by John Wiley & Sons Ltd.

However, rocking structures are often sufficiently flexible, especially in the lateral direction. For example, the piers of the South Rangitikei Rail Bridge in New Zealand^[2] are slender and laterally flexible, and were designed to rock on the bridge pile caps. Other examples of laterally flexible rocking objects include museum artefacts supported by relatively thin metallic rods on a free standing base and unanchored and thin-walled items of furniture. Furthermore, in recent years, the research community has been exploring the possibility of allowing buildings to rock on their foundations during earthquakes as a low damage design strategy. Such buildings would often behave as shear systems when fixed to their base, and hence cannot be considered to be rigid in the lateral direction. Therefore, it is necessary to relax the assumption of rigidity so that non-rigid rocking objects can be studied.

A number of studies^[3–10] have examined the dynamic behaviour of laterally flexible rocking objects using simple models. The objects that were examined were structural wall and frame systems with distributed masses. These systems were idealised with one or two concentrated masses, with the lower mass typically placed at ground level. These models are useful to understand the interactions between the vibration of the oscillator and the rocking motion, and will be referred to in this work as flexible rocking oscillators. Research^[3] has shown that the rocking motion has a significant influence on the vibration demands and that the vibrations may influence the stability of the structure. However, these behavioural trends are sensitive to the adopted impact models. A range of divergent assumptions were utilised to treat impact in flexible rocking oscillator models, and they are broadly categorised and discussed below.

During an impact between the flexible rocking oscillator and its support medium, both the angular velocity and the elastic translational velocity of the oscillator may change. If the impacting surfaces of the support medium and the rocking structure are rigid, impact can be assumed to occur instantaneously. To examine the rocking behaviour of buildings allowed to uplift, Meek^[4] and Chopra and Yim^[5] considered a flexible rocking oscillator with a single concentrated mass. They assumed an inelastic collision between the flexible rocking oscillator and the rigid support medium, always leading to a full contact phase where the post-impact angular velocity is zero. To estimate the post-impact elastic translational velocity of the oscillator, Meek^[4] postulated that the horizontal momentum of the oscillator is conserved during impact. This implies that no horizontal impulse acts on the oscillator during impact. Vassiliou et al.^[6] modelled the rocking response of a flexible column bolted to a base plate in contact with the support medium and carrying a steel weight at the top. They idealised this system with concentrated masses at the top and bottom of the flexible rocking oscillator. They assumed that the kinetic energy from the vertical component of pre-impact velocities is lost during impact. Similar to earlier work by Meek^[4] and Chopra and Yim,^[5] Vassiliou et al.'s^[6] approach always results in full contact phase upon impact. However, as will be shown later in the paper, this modelling approach is not consistent with the IPM. When stiff (effectively rigid) oscillators are considered, direct transitions to full contact at impact may lead to higher energy dissipation than the IPM.

By contrast, other studies additionally considered the possibility of transiting to a new rocking phase upon impact. Using single mass models, Oliveto et al.^[7] and Acikgoz and DeJong^[3] determined a post-impact phase (either full contact or rocking phase) by comparing the energy of possible phases and comparing the restraining moment and overturning moment at impact. In Acikgoz and DeJong's multi-mass model,^[8] the energy criterion is replaced by a momentum criterion. However, in both models,^[3,8] the elastic translational velocity of the oscillator is assumed to remain the same during a transition to rocking phase. Consequently, the horizontal momentum of the top mass is not conserved for these transitions, while it is conserved during transitions to full contact phase. This specific treatment of impact allowed Acikgoz and DeJong's models to yield near-identical results to the IPM for effectively rigid structures. However, as noted by Vassiliou et al.,^[6] Acikgoz and DeJong's approach can result in consecutive impacts for more flexible structures, leading to increased energy dissipation in the models.

Recent studies introduced impact models which only consider transition to a rocking phase upon impact. However, different assumptions were used to describe this transition. For instance, conservation of horizontal momentum of the oscillating mass was assumed by Cappelli et al.^[9] when studying the rocking behaviour of a masonry tuff wall. In contrast, when exploring posttensioned concrete rocking walls, Kalliontzis et al.^[10] assumed that velocities of the oscillator do not change during impact. Consequently, the horizontal momentum of the oscillating mass is not conserved in their model. It is interesting to note that Di Egidio et al.^[11] examined the effectiveness of the mass-damper absorber on rigid rocking block, which makes the whole system similar to a flexible rocking structure. Similar to Kalliontzis et al.'s treatment, a rocking transition is always made upon impact, while horizontal momentum of the absorber is not conserved. The wide range of modelling assumptions presented above highlights the need to develop more systematic criteria to describe post-impact transition to either full contact or rocking phases upon impact.

Additionally, most of the aforementioned flexible rocking models^[3,7–9] feature another assumption of the IPM: the locus of the vertical impulse is coincident with the future rocking corner. As a result, angular momentum is conserved about that corner when models transit from one rocking phase to another. This is a reasonable assumption for systems where the base of the rocking system has concentrated feet at its two bottom corners; the same approach will be adopted



in the current study. However, recent work by Chatzis et al.^[12] highlighted that the locus of impulse can be different from the future rocking corner. Different loci are admissible as long as impulsive forces remain under the base of the rocking system and lead to energy loss. A separate locus is indeed necessary for models to transition to full contact phase, but this has not been examined in previous research. To propose a general impact model that can account for varying impulse locus, the current study parametrises the position of impulse when developing the momentum equations. This enables the treatment of all phase transitions using the same momentum conservation laws.^[13]

It is noteworthy that previous studies on flexible rocking oscillators make further assumptions, similar to IPM, to simplify the treatment of impact. These assumptions are: the support medium is rigid, sliding and complete separation of the rocking structure from the support medium (free-flight behaviour) are neglected, and the motion of the system is assumed to be planar. Studies on rigid rocking models have shown that the deformability of the support medium,^[14–21] or sliding and free-flight behaviour^[19,22–25] or the 3D response of the rocking system^[26,27] can significantly affect the rocking response, and that neglecting them is not necessarily a conservative assumption. However, in this paper, the focus is on systems where the aforementioned aspects are expected to have a small influence. Therefore, similar to previous studies on flexible rocking oscillators, these mechanisms are neglected.

To propose a consistent and more generally applicable approach to model the dynamics of flexible rocking oscillators, this study proposes a new analytical model with two concentrated masses. The model geometry is defined such that the bottom mass can be placed above ground level; this contributes to generalising the analytical models to address structures where the rigid elements in contact with the support medium can assume a wide range of geometric properties. More importantly, a new impact modelling approach is introduced with the guiding principle that ideal springs and dampers cannot transmit impulses during an infinitesimally small duration impact. When combined with the possibility to consider the variable locus of impulse, a series of momentum equations emerge, which can uniquely determine the ensuing phase of motion and post-impact states. Section 2 presents the equations of motion of the new flexible rocking oscillator model, which considers a bottom mass at non-zero height and lumped rotational inertia. This is followed by the presentation of the new impact model. The equivalence of the new impact model to the IPM for effectively rigid structures is presented analytically in Section 3. Section 4 compares the rocking behaviour that results from the adoption of the new impact model and contrasts these results with other impact models. Free vibration time history results are shown and stability diagrams under pulse excitations are presented to illustrate how impact models influence dynamic behaviour. Section 5 presents a summary of findings, highlighting how the proposed impact model unifies the divergent assumptions from previous research within a consistent framework.

2 | ANALYTICAL MODEL

2.1 | Flexible rocking model

A new flexible rocking model (FRM) is developed, which consists of a rigid ‘U’ structure (bottom mass) and a top concentrated mass, as shown in Figure 1(A). To simplify the figure, the ‘U’ structure is represented as a box, but it can take any shape that is symmetric around the vertical line passing through the midpoint of the base of the ‘U’ structure. Point A is the centroid of the ‘U’ structure, which has a mass m_A and a mass moment of inertia I_A . Note the term bottom mass in the following refers to both the translational mass and rotational mass. The top mass is assumed to be a point mass, hence it has negligible rotational inertia. It is located at point P in its undeformed state.

The whole rocking system is referred to as the structure throughout the paper in order to distinguish it from its two parts (the ‘U’ structure and the top mass). The half-width of the structure is b . The centroid of the ‘U’ structure is at height h_A , and at a radial distance of R_A to corners o’ and o. The angle α_A ($\tan \alpha_A = b/h_A$) shown in Figure 1(A) will be referred to as the slenderness for this body. The top mass is connected to the ‘U’ structure with a spring (with stiffness, k) and a viscous damper (with damping coefficient, c). At rest, the height of the top mass is h , and it is located at a radial distance R from the corners. The top mass slenderness is denoted by α ($\tan \alpha = b/h$). Geometric parameters representing the centre of gravity (point C) of the undeformed structure are also illustrated in Figure 1(A). These are denoted with the subscript ‘cg’ where α_{cg} is the slenderness, h_{cg} is the height and R_{cg} is the radial distance of the centre of gravity from the corners.

The x - y coordinate system and its positive sign convention are shown in Figure 1(B), with o being the origin. Rotating axes x' and y' are also defined similarly with the same origin in the figure. The rocking angle θ is defined as the rotation that aligns the oxy axes to the $ox'y'$, with clockwise rotation being positive. The displacement of the top mass along the x' axis (referred to as elastic translational displacement) is defined as u . From Figure 1 onwards, viscous dampers will not be explicitly represented on the schematics to enable a cleaner visual representation of the model.



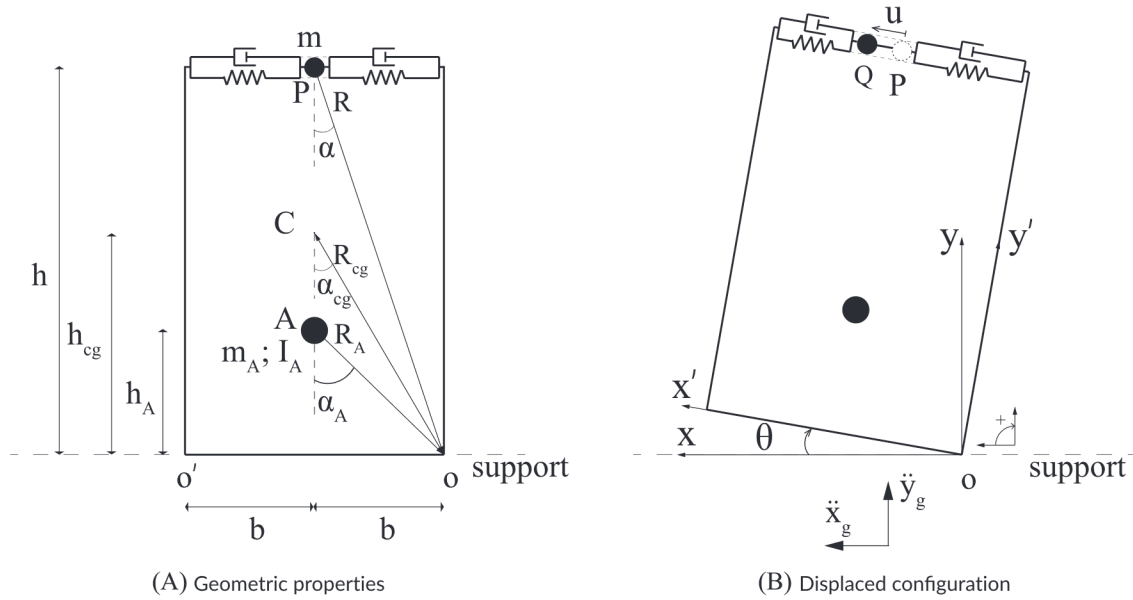


FIGURE 1 Flexible rocking model

The FRM considers three phases of motion: the full contact phase, the rocking phase with respect to o , and the rocking phase with respect to o' . The full contact phase corresponds to the two corners of the base of the 'U' structure being in contact with the support medium, and in rest, i.e. $\theta = 0$ and $\dot{\theta} = 0$. During the full contact phase, the top mass vibrates elastically parallel to the x axis. Its horizontal displacement u is the only degree of freedom. Figure 1(B) illustrates the motion of the FRM when the structure is rocking with respect to the right corner o . In this phase, the structure is pivoting about the right corner o while the top mass moves laterally, i.e. along the direction of x' , with a displacement u displacing it from point P (the location of the mass when the spring is undeformed) to point Q .

For all the three phases of motion, the kinematics of the centroid of the 'U' structure (point A) and the centroid of the top mass (point Q) can be expressed by Equations (1)–(4) using the degrees of freedom θ and u . They describe the position of masses in the xy coordinate system, where the upper sign refers to rocking around the right corner o and the lower sign refers to rocking around the left corner o' . For full contact phase, either the upper sign or the lower sign can be used. Here x_A, y_A are the horizontal and vertical coordinates of point A ; x_Q, y_Q are the horizontal and vertical coordinates of point Q .

$$x_A = b \mp b \pm R_A \sin(\alpha_A \mp \theta) \quad (1)$$

$$y_A = R_A \cos(\alpha_A \mp \theta) \quad (2)$$

$$x_Q = b \mp b \pm R \sin(\alpha \mp \theta) + u \cos \theta \quad (3)$$

$$y_Q = R \cos(\alpha \mp \theta) + u \sin \theta \quad (4)$$

This study considers cases where sliding and free-flight would not occur, and hence these aspects are not modelled. The FRM is similar to models from previous studies^[3–7] which adopted an inverted 'T' shape to describe the flexible rocking oscillators. The 'U' representation was preferred in this study instead as this shape explicitly defines the spring and viscous damper elements, and conceptually clarifies the need to consider a bottom mass with non-zero height and mass moment of inertia. The 'U' shape is an abstraction, it can be used to represent any vertically symmetric rigid object that connects the flexible spring and damper to the rigid support medium.

2.2 | Equations of motion

The FRM is subjected to horizontal (\ddot{x}_g) and vertical (\ddot{y}_g) ground accelerations as shown in Figure 1(B). Although vertical ground acceleration terms are presented for completeness, the influence of vertical accelerations will not be investigated

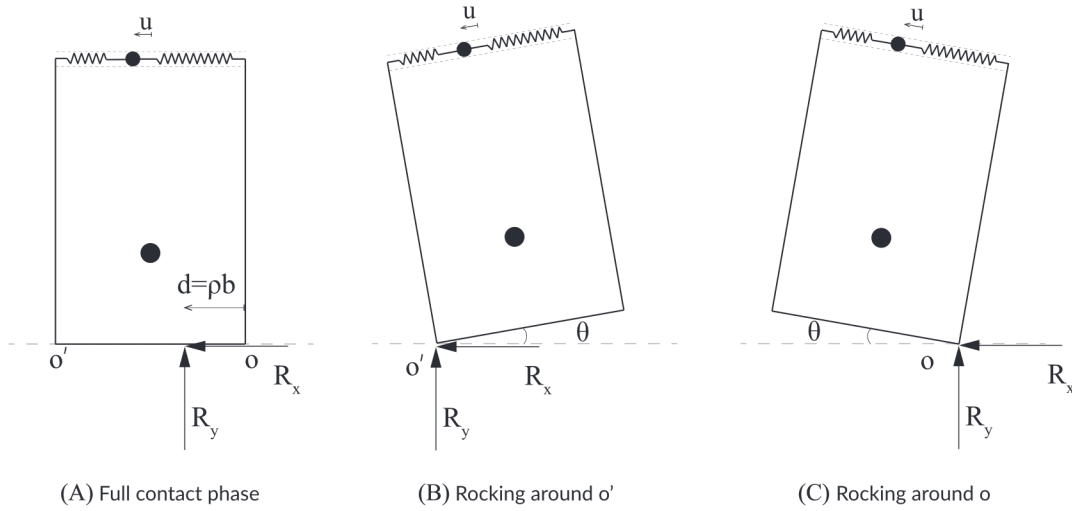


FIGURE 2 Reaction forces R_x and R_y during different phases of motion

in this paper, since the focus of this study is to characterise the influence of impact laws on structural response with basic excitation patterns. The horizontal equation of motion that describes the full contact phase of the FRM is:

$$\ddot{u} + \frac{c}{m}\dot{u} + \frac{k}{m}u = -\ddot{x}_g \quad (5)$$

where each dot over a symbol indicates a time derivative operator. In Equation (5), $\frac{c}{m}$ and $\frac{k}{m}$ can be replaced by $2\zeta_n\omega_n$ and ω_n^2 , where ζ_n is the damping ratio and ω_n is the natural frequency of the oscillator with mass m .

The equations of motion for the rocking phases are expressed as follows:

$$\ddot{u} - h\ddot{\theta} + (\mp b - u)\dot{\theta}^2 + \frac{c}{m}\dot{u} + \frac{k}{m}u = -\ddot{x}_g \cos \theta - (\ddot{y}_g + g) \sin \theta \quad (6)$$

$$[I_A + m_A R_A^2 + m(R^2 + u^2 \pm 2bu)]\ddot{\theta} - m h \ddot{u} + 2m(\pm b + u)\dot{u}\dot{\theta} - m(\ddot{y}_g + g)[\mp R \sin(\alpha \mp \theta) - u \cos \theta] \pm m_A(\ddot{y}_g + g)R_A \sin(\alpha_A \mp \theta) = m\ddot{x}_g[R \cos(\alpha \mp \theta) + u \sin \theta] + m_A\ddot{x}_g R_A \cos(\alpha_A \mp \theta) \quad (7)$$

where the upper sign refers to rocking around the right corner o and the lower sign refers to rocking around the left corner o' . In addition, g denotes the gravitational acceleration, which will be taken in this paper as 9.81 m/s^2 . Equations (6) and (7) describe equilibrium of the top mass along x' axis and the rotational equilibrium of the system with respect to the rocking corner, respectively.

2.3 | Uplift

The first type of transition examined is from full contact phase to a rocking phase, i.e. uplift. Uplift occurs when the reaction forces exerted by the support medium on the structure during the full contact phase become coincident with one of the corners o and o' (see Figures 2(B) and 2(C)).

The support forces R_x and R_y (the horizontal and vertical reaction force respectively applied by the support medium to the 'U' structure) during a full contact phase are schematically illustrated in Figure 2(A). The horizontal position of R_y from the origin is denoted by d , with its positive direction being along x axis. It is useful to normalise this position by the half-width b to obtain a dimensionless position variable, denoted by ρ . During full contact, the horizontal position of the reaction force R_y can then be expressed as follows:

$$\rho = 1 - \frac{m_A \ddot{x}_g h_A - m(\ddot{y}_g + g)u - (ku + c\dot{u})h}{(m_A + m)(\ddot{y}_g + g)b} \quad (8)$$

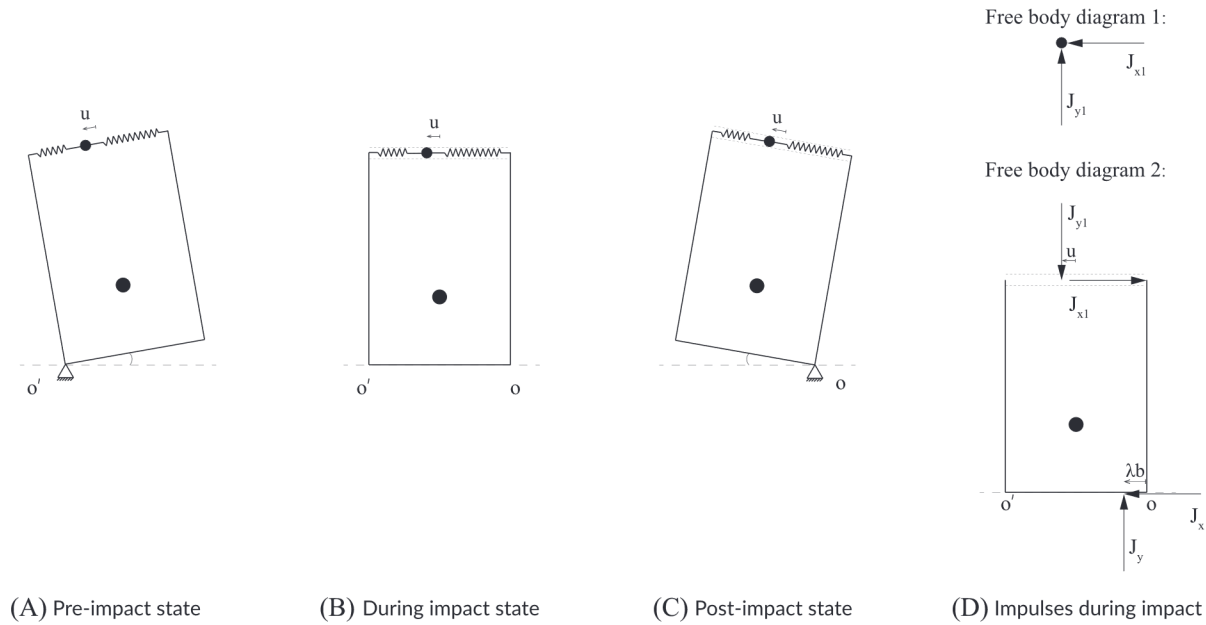


FIGURE 3 The process of impact at the right corner

To initiate rocking motion about the right and left corners, ρ needs to assume the values of 0 and 2, respectively. This condition is expressed as follows:

$$\mp(\rho - 1) = 1 \quad (9)$$

where the upper and lower signs refer to a transition towards rocking around the right corner and rocking around the left corner, respectively. Equation (9) can be used to determine the critical displacement u_{cr} , which is the specific elastic translational displacement when uplift happens. According to Equations (8) and (9), u_{cr} is dependent on \ddot{x}_g and \ddot{y}_g unless $h_A = 0$. In order to get a critical displacement that can be conveniently used to normalise u , the u_{cr} of a structure with zero bottom mass height ($h_A = 0$) and no damping is utilised as defined in Equation (10).

$$u_{cr} = \pm \frac{\frac{m_A+m}{m}gb}{\omega_n^2 h} \quad (10)$$

2.4 | Impact

The second type of phase transition occurs when $\theta = 0$ and $\dot{\theta} \neq 0$ (see Equation (11)) and involves an impact between the structure and its support medium. A new impact model (called Impact Model 1 or IM1) is developed and compared to existing impact modelling approaches from the literature.

$$\theta = 0, \dot{\theta} \neq 0 \quad (11)$$

2.4.1 | Impact model 1 (IM1)

For brevity, the figures in this section illustrate the FRM transiting from rocking with respect to the left corner o' to rocking with respect to the right corner o (i.e. impact at the right corner o), while the equations are presented for impacts at both corners. The FRM model is illustrated in Figure 3(A) in its pre-impact state and in Figure 3(C) in its post-impact state, with exaggerated rocking angles for clarity. During impact, the FRM model is shown in Figure 3(B), and two set of impulsive forces occur. The first set of impulsive forces is between the base of the 'U' structure and the support medium, while the

second set is between the 'U' structure and the top mass. Figure 3(D) shows the free body diagrams of the top mass and the 'U' structure, where the resultant impulses are illustrated. J_x and J_y are the horizontal and vertical impulse applied by the support medium to the 'U' structure. J_{x1} and J_{y1} are the horizontal and vertical impulse between the 'U' structure and the top mass.

J_x and J_y are impulses arising from the collision of two rigid objects, namely the 'U' structure and the support medium. As both bodies are rigid, the impact has an infinitesimal duration. During this impact, the impulsive forces applied by the support medium to the 'U' structure are of an impulsive nature, i.e. they correspond to Dirac delta functions. Consequently, despite the fact the duration of the impact tends to zero, these forces produce non-zero impulses. On the other hand, J_{x1} and J_{y1} describe the interaction between the top mass and the 'U' structure. These two components are rigidly connected in the vertical direction. As a result, J_{y1} also assumes some non-zero value. However, the top mass and the 'U' structure are connected horizontally through a spring and a damper. As the duration of the impact is infinitesimally small, the elongation of the spring does not change during impact. As a result, the force of the spring remains finite and the corresponding impulse produced over this impact of infinitesimal duration will be zero. Similarly the velocity of the mass changes in a step-manner during the impact and hence the force of the damper remains finite. Hence neither the spring, nor the damper generate a horizontal impulse, leading to $J_{x1} = 0$.

To determine the post-impact velocities of the FRM, the locations of the impulses need to be considered. J_{y1} acts at the centroid of the top mass but a range of plausible positions exist for the horizontal location of J_y .^[12] To take this into account, the vertical location of J_y is parametrised to be λb measured from the future rocking corner. For positive values of λ between 0 and 2, the impulse remains under the base of the 'U' structure (see Figure 3(D)). The momentum equations are then developed as a function of λ . Since the impulses are expressed along the x and y axes, the translational momentum conservation equations are expressed around the same directions. Having produced a free body diagram for each of the rigid bodies (the top mass and the 'U' structure) in Figure 3(D), the translational momentum equations are presented in terms of these two bodies. For convenience, the angular momentum conservation for the 'U' structure is written around the centroid of the 'U' structure:

$$m\dot{x}_Q^+ = m\dot{x}_Q^- \quad (12)$$

$$m\dot{y}_Q^+ = m\dot{y}_Q^- + J_{y1} \quad (13)$$

$$m_A\dot{x}_A^+ = m_A\dot{x}_A^- + J_x \quad (14)$$

$$m_A\dot{y}_A^+ = m_A\dot{y}_A^- + J_y - J_{y1} \quad (15)$$

$$I_A\dot{\theta}^+ = I_A\dot{\theta}^- - J_{y1}u \mp J_y(b - \lambda b) + J_x h_A \quad (16)$$

where \dot{x}_Q , \dot{y}_Q denote the horizontal and vertical velocities of the top mass, \dot{x}_A , \dot{y}_A denote the horizontal and vertical velocities of the centroid of the 'U' structure, and $\dot{\theta}$ is the angular velocity. The superscripts $-$ and $+$ indicate the pre- and post-impact quantities. The upper and lower signs refer to impact at the right corner and the left corner, respectively. A similar notation is used consistently in this paper to describe impact. The velocities at the points Q and A can be expressed in terms of the degrees of freedom \dot{u} and $\dot{\theta}$, by considering the pre- and post-impact kinematic constraints (see Equations (1)–(4)). Five equations emerge (Equations (12)–(16)) to solve the six unknowns (J_x , J_y , J_{y1} , $\dot{\theta}^+$, \dot{u}^+ and λ). To find the post-impact velocities, it is necessary to assume a value for λ . This yields $\dot{\theta}^+$ and \dot{u}^+ in the following compact form:

$$\dot{\theta}^+ = e\dot{\theta}^- \quad (17)$$

$$\dot{u}^+ = \dot{u}^- - h\dot{\theta}^-(1 - e) \quad (18)$$

where e is the coefficient of restitution for angular velocity. It is expressed by Equation (19):

$$e = \frac{\dot{\theta}^+}{\dot{\theta}^-} = \frac{I_A + m_A h_A^2 + mu(\mp b + u) + b(1 - \lambda)(-m_A b - mb \pm mu)}{I_A + m_A h_A^2 + mu(\pm b + u) + b(1 - \lambda)(m_A b + mb \pm mu)} \quad (19)$$

The above discussion presents equations to calculate the post-impact velocities for potential full contact and rocking phases after impact. In the proposed impact model IM1, results from these equations are used to determine the post-impact phase. First, a chosen value of λ (denoted as λ_c) is used to calculate the coefficient of restitution $e(\lambda_c)$ according to Equation (19). A post-impact transition to rocking can be made if $e(\lambda_c) > 0$. However, if $e(\lambda_c) < 0$, a post-impact rocking phase is unfeasible as the pre-impact corner would penetrate the rigid support medium. In this case, a new λ (denoted as λ_{new}) needs to be used to replace λ_c and to obtain the a new coefficient of restitution $e(\lambda_{new})$. $e(\lambda_{new})$ must be greater than zero if a new rocking phase is to follow, or $e(\lambda_{new}) = 0$ if the post-impact phase is the full contact phase. Thus for either of the two allowable post-impact phases:

$$e(\lambda_{new}) \geq 0 \quad (20)$$

In this study, it is suggested that the nearest allowable value λ to the originally chosen λ_c is used in order to satisfy Equation (20). In the conference paper,^[13] it has been shown that e is monotonically increasing with λ , thus the nearest λ that meets $e(\lambda_{new}) \geq 0$ is the one that makes e zero, which is defined as λ_0 (i.e. $e(\lambda_0) = 0$).

Therefore, for cases where Equation (19) results in $e(\lambda_c) < 0$, the new λ is set λ_0 . In other words, the rocking phase is rejected as a post-impact phase, and instead a full contact phase follows the impact since $e(\lambda_0) = 0$ and the post-impact angular velocity is zero. This treatment of transiting to a full contact phase when the sign of the angular velocity is reversed coincides with the routinely used method in the work of Spanos and Roussis,^[28] and Chatzis et al.^[29] The conference paper^[13] provided an explanation for this treatment by comparing the λ required for this full contact pattern to occur in comparison to the values of λ needed to avoid the reversal of the sign of the angular velocity during impact and showing that the former is not greater than the latter. This provides an argument that for such cases, and under the assumptions of pure rocking before and after impact, the full contact scenario would result in a value of λ closer to the one originally assumed, which in this paper is set to $\lambda = 0$. Under the further argument that care has been provided to ensure that the λ assumed is the one more likely to occur during the experiment, i.e. by placing feet on the rocking structure, then it can be reasonably argued that the consideration of full contact after impact for such cases is reasonable.

The criterion for deciding the post-impact phase has been explained as above. However, another criterion needs to be added for the stability of the numerical implementation. Even if $e(\lambda_c) > 0$, a full contact phase is enforced when the post-impact angular velocity is extremely small, which means the rocking motion is practically about to stop. The transition criteria are expressed by Equations (21)–(22).

$$e(\lambda_c) > 0 \quad (21)$$

$$|\dot{\theta}^+| > \dot{\theta}_{min} \quad (22)$$

where $\dot{\theta}_{min}$ is the minimal angular velocity, chosen as 10^{-9} . This value is associated with small rotational kinetic energy, that is typically observed at impacts for very small rocking motion. A transition to rocking phase is made if both of them are met, otherwise a full contact transition follows.

It is insightful to note that the post-impact velocities of both a rocking transition and a full contact transition can be expressed by Equations (17) and (18), except that $e = 0$ for a full contact transition. For clarity, the post-impact velocities of a full contact transition is rewritten in Equations (23) and (24).

$$\dot{\theta}^+ = 0 \quad (23)$$

$$\dot{u}^+ = \dot{u}^- - h\dot{\theta}^- \quad (24)$$

As such, the transition to full contact phase can be viewed as a phase transition where a different locus of J_y (defined as λ_0) is implicitly chosen to yield $e = 0$. λ_0 can be found by setting Equation (19) to zero and rearranging:

$$\lambda_0 = 1 + \frac{(I_A + m_A h_A^2) + mu(\mp b + u)}{b(-m_A b - mb \pm mu)} \quad (25)$$

Equation (25) shows that a transition to full contact requires a specific locus of J_y . This observation justifies the choice to proceed to a new rocking phase whenever possible. The full contact phase transition only occurs when the rocking motion is not kinematically admissible for the chosen locus of J_y (i.e. λ_c).

According to Equation (19), it is noteworthy that a wide range of possible values for e exist when the range of plausible values of λ_c are considered. This makes IM1 a versatile impact model that can numerically evaluate the experimentally observed variability of energy dissipation at impact. However, as mentioned in the introduction, λ_c will be taken as zero, whenever possible. This corresponds to an impact locus at the future rocking corner and is of special interest for the wide range of structures designed to rock on dedicated feet. Hence this corresponds to the usual assumption made in the literature that the angular momentum of the structure would be conserved about the future rocking corner during impact. This position also corresponds to the impact locus chosen by Housner to calculate energy dissipated at impact and presents an important benchmark. The influence of adopting different values of λ_c has been explored in the conference paper^[13]; interested readers are referred to this publication for further details.

The new impact model (IM1) has been presented in this section, and the next two sections will be devoted to two other impact models from the literature for comparison.

2.4.2 | Impact model 2 (IM2)

Acikgoz and DeJong's model^[3] (denoted by IM2) is chosen for comparison as it yields near-identical results to the IPM for very stiff (effectively rigid) structures and is numerically stable. As discussed in the introduction, IM2 assumes a non-zero J_{x1} for transition to rocking phase and a zero J_{x1} for transition to full contact phase. The following two conditions are required for a post-impact transition to a rocking phase, instead of full contact, with the first equation examining the angular momentum ($\pm L^-$) about the future rocking corner, while the second equation being used to ensure numerical stability:

$$\pm L^- = \pm\{-mh\dot{u}^- + [mh^2 - (m + m_A)b^2 + mu^2 + I_A + m_A h_A^2]\dot{\theta}^-\} > 0 \quad (26)$$

$$|\dot{\theta}^+| > \dot{\theta}_{min} \quad (27)$$

- Transition to a rocking phase

If both Equations (26) and (27) are satisfied, then the structure will proceed with a new rocking phase. Since J_{x1} is non-zero, there are five momentum equations with seven unknowns (J_x , J_y , J_{x1} , J_{y1} , $\dot{\theta}^+$, \dot{u}^+ and λ). Hence, an additional assumption must be introduced. That assumption is that the elastic translational velocity of the oscillator does not change during impact ($\dot{u}^+ = \dot{u}^-$). Furthermore, λ is assumed to be 0. This yields the following post-impact velocities:

$$\dot{\theta}^+ = e\dot{\theta}^- \quad (28)$$

$$\dot{u}^+ = \dot{u}^- \quad (29)$$

e is given by Equation (30), which is different from Equation (19) because of the non-zero value of J_{x1} . Note that Equation (30) always yields a greater e than Equation (19) for the same pre-impact conditions.

$$e = \frac{I_A + m_A h_A^2 + mh^2 + mu(\mp b + u) + b(1 - \lambda)(-m_A b - mb \pm mu)}{I_A + m_A h_A^2 + mh^2 + mu(\pm b + u) + b(1 - \lambda)(+m_A b + mb \pm mu)} \quad (30)$$

- Transition to the full contact phase

If either of the conditions in Equations (26) and (27) is not met, a full contact phase follows. The initial velocities of the new full contact phase are the same as Equations (23) and (24) as J_{x1} is assumed to be zero for this transition.



TABLE 1 Π groups

Π groups	Π_1	Π_2	Π_3	Π_4	Π_5	Π_6	Π_7	Π_8	Π_9	Π_{10}
Quantity	ω_n/p	ζ_n	α_{cg}	α_A	ω/p	$A/(g \tan(\alpha_{cg}))$	pt	m_A/m	$I_A/(m_A R_A^2)$	λ

2.4.3 | Impact model 3 (IM3)

As discussed in the introduction, a number of flexible rocking oscillator models^[4–6] always choose a transition to full contact following an impact. Impact model 3 (denoted by IM3) corresponds to the modelling assumptions of forcing a full contact phase after an impact, i.e. $\dot{\theta}^+ = 0$. The assumption of conservation of horizontal momentum of the top mass is also used, i.e. $J_{x1} = 0$. With these assumptions, IM3 becomes a special case of IM1, where the post-impact parameters of the new full contact phase are given by Equations (23) and (24). It is important to note that this transition implies an impact locus of λ_0 , defined earlier in Equation (25). This value is not constant for a structure as it depends on the elastic translational displacement u at the time of impact. Furthermore, it should be emphasised that in IM3, λ_0 may assume inadmissible value where the impulse loci may not be located under the base of the structure. Finally, it is also worth noting that for stiff structures, IM3 does not converge to the IPM, as will be shown later in this paper.

2.5 | Dimensional analysis

In order to systematically study the FRM, dimensional analysis for the response of the system subjected to single cycle sinusoidal pulse excitations is informative^[30] and thus employed in this study. Only horizontal excitations are considered here (i.e. $\ddot{y}_g = 0$) and they are given by Equation (31).

$$\ddot{x}_g = \begin{cases} A \sin(\omega t) & t \leq 2\pi/\omega \\ 0 & t > 2\pi/\omega \end{cases} \quad (31)$$

where A and ω denote the amplitude and angular frequency of the pulse.

The rocking responses under such excitations can be expressed with 13 parameters:

$$(u, \theta) = f(\omega_n, \zeta_n, \alpha, \alpha_A, \omega, A, t, m, m_A, I_A, g, b, \lambda) \quad (32)$$

There are three fundamental dimensions (length, force and time) involved. According to Buckingham's Π theorem,^[31] the two non-dimensional response parameters can be expressed by $13 - 3 = 10$ non-dimensional parameters. Three repeating parameters (p , g and m) and ten Π groups were chosen (shown in Table 1). The equations of motion and impact equations can be expressed by these Π groups. The two response parameters (chosen as u/u_{cr} and θ/α_{cg}) can be expressed by the following formula. Note that p is the frequency parameter for rocking ($p = \sqrt{(m + m_A)gR_{cg}/(I_A + m_A R_A^2 + mR^2)}$).

$$(u/u_{cr}, \theta/\alpha_{cg}) = f(\omega_n/p, \zeta_n, \alpha_{cg}, \alpha_A, \omega/p, A/(g \tan \alpha_{cg}), pt, m_A/m, I_A/(m_A R_A^2), \lambda) \quad (33)$$

A script was written in MATLAB (MathWorks, 2019) to carry out the simulation of the FRM with the three different impact models (IM1, IM2 and IM3) introduced earlier. The equations of motion were integrated over time using the ordinary differential equation (ODE) solver ode45, which corresponds to a variable time-stepping Runge–Kutta 4–5 pair.^[32] The phase transitions (see Equations (9) and (11)) were detected using the the ODE solver's event-detection scheme.

3 | THE BEHAVIOUR OF IM1 FOR RIGID STRUCTURES

It is interesting to compare the new impact model IM1 with established models of energy dissipation, such as the IPM, for in the limit of the spring becoming infinitely stiff, i.e. for effectively rigid structures.



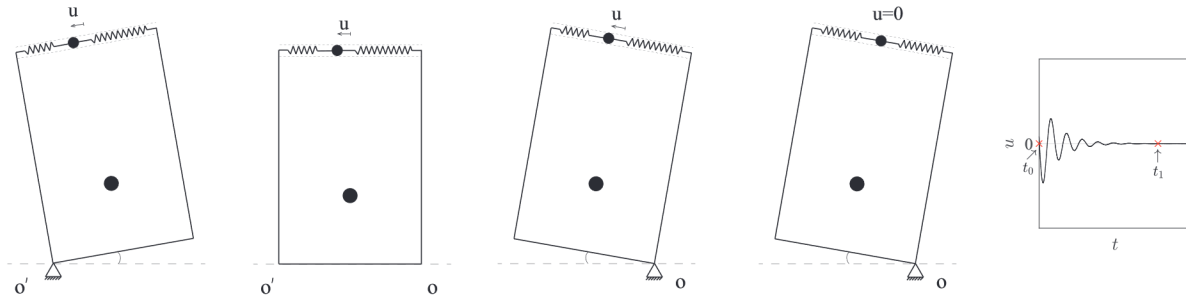


FIGURE 4 The process of impact at the right corner for IM1 for an effectively rigid structure

The coefficient of restitution for the IM1 model of the FRM was given in Equation (19). For an effectively rigid structure, prior to impact $u = 0$ and $\dot{u} = 0$. It is further assumed that $\lambda = 0$ as in the IPM.^[1] Those lead to the following expression:

$$e_{IM1} = \frac{I_A + b(-m_A b - mb) + m_A h_A^2}{I_A + b(+m_A b + mb) + m_A h_A^2} \quad (34)$$

where e_{IM1} refers to the coefficient of restitution calculated by IM1 for the effectively rigid structure.

On the other hand, the coefficient of restitution for the IPM, which has the same geometry of the FRM structure, can be expressed by the following equation.

$$e_{IPM} = \frac{I_A + b(-m_A b - mb) + m_A h_A^2 + mh^2}{I_A + b(+m_A b + mb) + m_A h_A^2 + mh^2} \quad (35)$$

It is interesting to note that the exact same expression in Equation (35) can be obtained by substituting $u = 0$ and $\lambda = 0$ into Equation (30), which is the coefficient of restitution for IM2 model. This observation reveals that Equation (35) considers the transfer of horizontal impulse during impact (a non-zero J_{x1}). Indeed, in the case of a rigid structure the two masses would also be connected through a rigid link that would be capable of passing impulses during an infinitesimally small duration impact.

It is clear that the coefficients of restitution for IM1 (e_{IM1}) and the IPM (e_{IPM}) are different. However, IM1 additionally considers energy transfer to the oscillator, which needs to be evaluated to understand the total energy dissipation occurring at impact and just after it. In order to analyse the impact of IM1 in detail, four instants are examined as shown in Figures 4(A)–4(D): the pre-impact instant ($t = t_0^-$), the during impact instant ($t = t_0$), the post-impact instant ($t = t_0^+$) and the instant at which the spring stops deforming ($t = t_1$). The second (t_0) and fourth instants (t_1) are illustrated in Figure 4(E), which shows an indicative time history of u . The time increment from t_0 to t_1 tends to zero for rigid structures, i.e. as $k \rightarrow \infty$. The same assumption requires that $c \rightarrow \infty$ for the elastic translational displacement u to decay. During this infinitesimally small duration, the value of θ does not change. In contrast, u decays as the spring experiences rapid oscillations. The overall time duration of the whole process in Figure 4 also tends to zero.

There are six velocities that are going to be used in the following derivation: $\dot{\theta}_{t_0^-}$, $\dot{u}_{t_0^-}$, $\dot{\theta}_{t_0^+}$, $\dot{u}_{t_0^+}$, $\dot{\theta}_{t_1}$, \dot{u}_{t_1} , which correspond to the values of $\dot{\theta}$ and \dot{u} at three different instants (t_0^- , t_0^+ and t_1) as indicated by their subscripts. Similarly, there are six values of θ and u defined at the same time instances: $\theta_{t_0^-}$, $u_{t_0^-}$, $\theta_{t_0^+}$, $u_{t_0^+}$, θ_{t_1} , u_{t_1} . After defining these instants, and related velocities and displacements, the equations of motion (Equations (6) and (7)) are used to analyse the rocking behaviour of the structure just after impact (from t_0^+ to t_1) in IM1. Furthermore, as k and $c \rightarrow \infty$, all the terms that do not involve k , c or the accelerations of the system $\ddot{\theta}$ and \ddot{u} will be negligible and can be neglected. This results in neglecting the gravitational, external forces and terms involving products of the velocities. As $\theta = 0$ during the studied interval, the following equations are obtained:

$$\ddot{u} - h\ddot{\theta} + \frac{c}{m}\dot{u} + \frac{k}{m}u = 0 \quad (36)$$

$$-mh\ddot{u} + (I_A + m_A R_A^2 + mR^2)\ddot{\theta} = 0 \quad (37)$$

After substituting Equation (36) into Equation (37), and assuming that the movement of the top mass is under-damped, analytical solution of u can be obtained:

$$u = \frac{\dot{u}^+}{\gamma} e^{\beta t} \sin \gamma t \quad (38)$$

where $\beta = -\omega\zeta/\delta$, $\gamma = \omega\sqrt{\delta - \zeta^2}/\delta$, $\delta = 1 - mh^2/(I_A + m_A R_A^2 + mR^2)$. Equation (38) shows how the top mass oscillates quickly before the motion stops.

The value of $\dot{\theta}_{t_1}$ can be found by integrating Equation (37) over the time period t_{0+} to t_1 :

$$\dot{\theta}_{t_1} = \frac{mh(\dot{u}_{t_1} - \dot{u}_{t_{0+}})}{I_A + m_A R_A^2 + mR^2} + \dot{\theta}_{t_{0+}} \quad (39)$$

According to Equations (17) and (18), $\dot{\theta}_{t_{0+}} = e_{IM1}\dot{\theta}_{t_{0-}}$, $\dot{u}_{t_{0+}} = \dot{u}_{t_{0-}} + h\dot{\theta}_{t_{0-}}(e_{IM1} - 1)$. Since the motion of the spring stops at t_1 , $\dot{u}_{t_1} = 0$, $\dot{u}_{t_{0-}} = 0$. By substituting these quantities into Equation (39) and referring to Equations (34) and (35), $\dot{\theta}_{t_1}$ can be obtained as follows.

$$\dot{\theta}_{t_1} = e_{IPM}\dot{\theta}_{t_{0-}} \quad (40)$$

Since the stiffness of the spring is infinite, the time needed for the elastic translational displacement to cease is zero, i.e. $t_1 - t_{0+} = 0$. Thus, Equation (40) shows that the angular velocity changes from the pre-impact value $\dot{\theta}_{t_{0-}}$ to the post-impact value $e_{IM1}\dot{\theta}_{t_{0-}}$ before changing again to $e_{IPM}\dot{\theta}_{t_{0-}}$ during an infinitesimally small period $t_1 - t_{0+}$. Therefore the energy dissipated by IM1 during impact for effectively rigid structures is identical to the energy dissipated by the IPM with the same geometry. This finding will be evaluated numerically in the next section.

4 | IMPACT MODEL COMPARISON

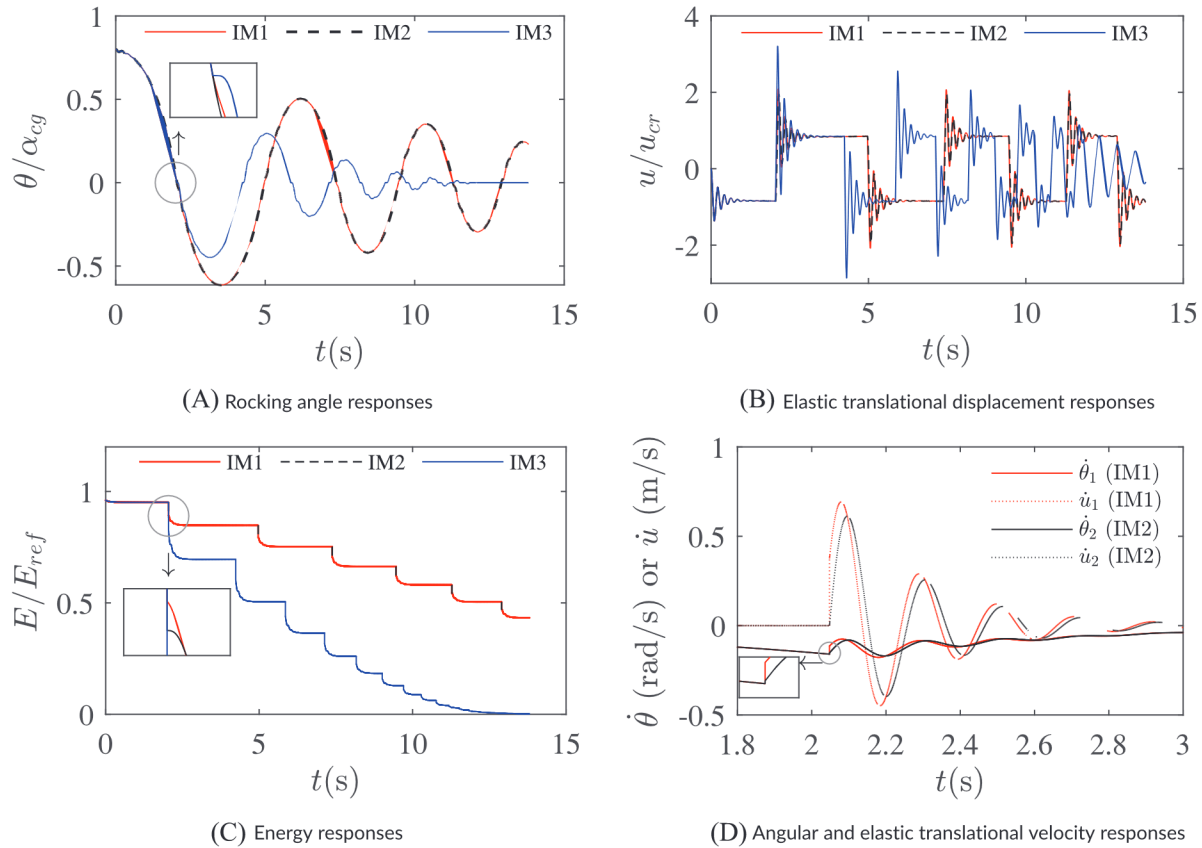
This section presents numerical results to compare the three impact models. Free vibration behaviour is examined with three different FRM geometries to obtain insight into how different impact models dissipate energy and understand how they influence the vibrations induced at impact. Trigonometric pulses have been used in previous studies to examine the stability of rocking structures.^[33,34] The same approach is followed in this study to systematically clarify the influence of the investigated impact models on the stability of flexible structures. Note again that the impact locus is assumed to be the future rocking corner whenever possible.

4.1 | Free vibration response

Free vibration simulations are conducted in this section to compare the response of the system when using the aforementioned three impact models. The FRM can be used to address a wide range of geometries. A review of studies in the literature by Acikgoz and DeJong^[34] suggests that rocking civil engineering structures are generally slender and have frequency parameter values smaller than 1.5 s^{-1} . These structures may have appreciable bottom mass with non-zero height due to their foundations. To this end, a slenderness value of $\alpha_{cg} = 0.1476$ was initially chosen with significant bottom mass ($m_A/m = 0.4746$), although more stocky geometries ($\alpha_{cg} = 0.2500$) and other bottom mass cases ($m_A/m = 0$ and $h_A = 0$) will be examined later in the paper. The common geometric parameters used for the free vibration simulations are summarised in Table 2 and can be envisioned to represent a small elevated water tank. To obtain insight into the influence of impact models on dynamic behaviour, three examples, each with a unique stiffness of the spring, were explored (Example 1: $\omega_n = 9.8225p$, Example 2: $\omega_n = 4.9599p$, Example 3: $\omega_n = 2.4313p$). Examples 1 and 3 represent rigid and very flexible structures, while Example 2 has a vibration period of 1.1 s, a reasonable estimate for a structure of this size. Similar dimensionless parameters were adopted in earlier work by Acikgoz and DeJong.^[3] The response of the system for the three examples is shown in the following Figures 5–7, respectively.

TABLE 2 Common parameters of free vibration simulations for Examples 1–3

Parameter	Value	Parameter	Value	Parameter	Value
$h(\text{m})$	8.2933	$h_A(\text{m})$	3.4250	$h_{cg}(\text{m})$	6.7263
$R(\text{m})$	8.3534	$R_A(\text{m})$	3.5680	$R_{cg}(\text{m})$	6.8003
$\alpha(\text{rad})$	0.1200	$\alpha_A(\text{rad})$	0.2841	$\alpha_{cg}(\text{rad})$	0.1476
$b(\text{m})$	1.0000	$I_A(\text{kg}\cdot\text{m}^2)$	1.1297×10^5	$p(\text{s}^{-1})$	1.1143
$m(\text{kg})$	3.3173×10^4	$m_A(\text{kg})$	1.5746×10^4	ζ_n	0.0500

**FIGURE 5** Example 1: free vibration responses of a stiff structure ($\omega_n = 9.8225p$)

In Figures 5–7, the dimensionless energy response is presented, which is defined by E/E_{ref} , where E is the total energy and E_{ref} is the potential energy difference between the unstable and stable equilibrium of the system, as defined in Acikgoz and DeJong.^[3] E and E_{ref} are defined, for the case of a support medium that moves in the x direction, through the following equations:

$$E = T_A + T + V \quad (41)$$

$$T_A = \frac{1}{2}(J_A + m_A R_A^2)\dot{\theta}^2 + \frac{1}{2}m_A \dot{x}_g^2 - \frac{1}{2}m_A(2\dot{x}_g R_A \cos(\alpha_A \mp \theta)\dot{\theta}) \quad (42)$$

$$T = \frac{1}{2}m \left[(R^2 + u^2)\dot{\theta}^2 + \dot{u}^2 - 2h\dot{\theta}\dot{u} \pm 2bu\dot{\theta}^2 + \dot{x}_g^2 - 2\dot{x}_g R \cos(\alpha \mp \theta)\dot{\theta} + 2\dot{x}_g \dot{u} \cos \theta - 2\dot{x}_g u \dot{\theta} \sin \theta \right] \quad (43)$$

$$V = mg[R \cos(\alpha \mp \theta) + u \sin \theta] \pm m_A g b \sin \theta + m_A g h_A \cos \theta + \frac{1}{2}k u^2 \quad (44)$$

$$E_{ref} = m_A g R_A \cos(\alpha_A - \alpha_{cg}) - m_A g h_A + mg R \cos(\alpha_{cg} - \alpha) - mgh \quad (45)$$

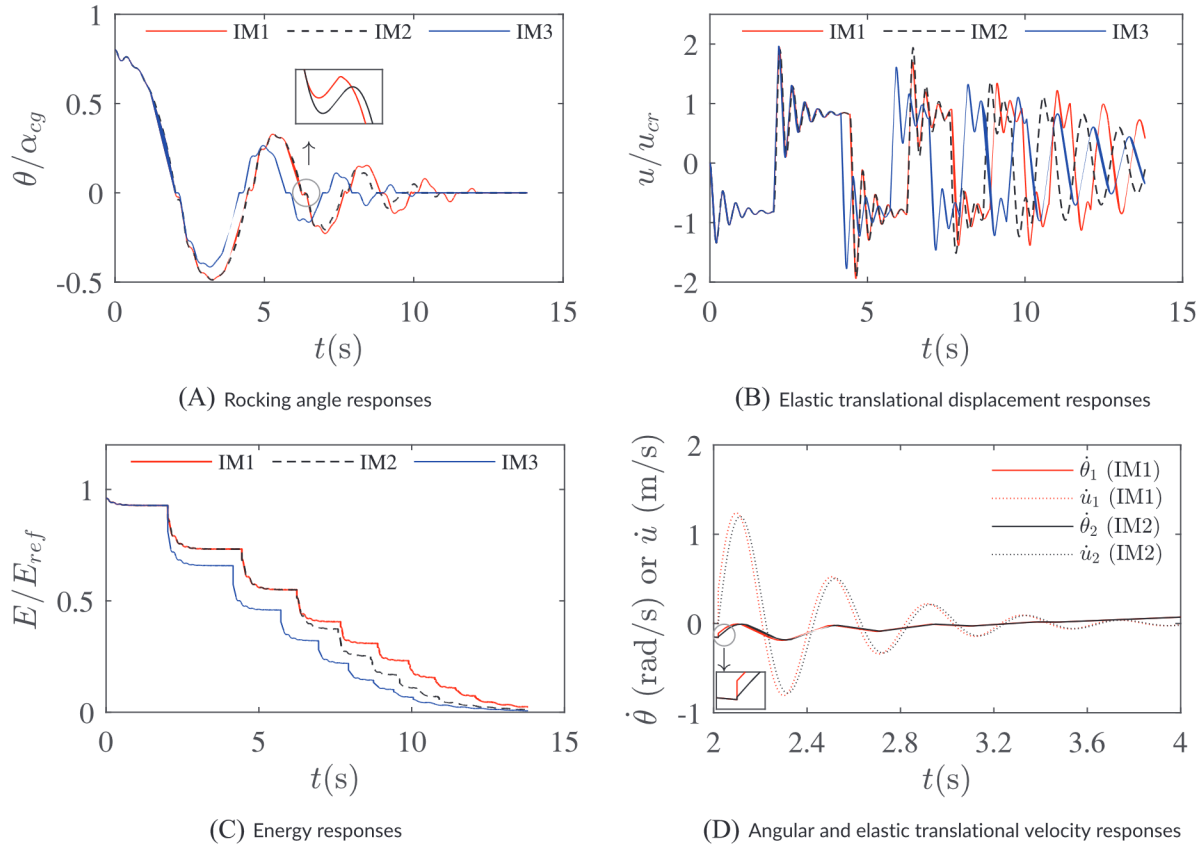


FIGURE 6 Example 2: free vibration responses of an intermediately stiff structure ($\omega_n = 4.9599p$)

where T_A is the kinetic energy of the ‘U’ structure, T is the kinetic energy of the top mass, V is the potential energy of the system. Here the upper sign refers to rocking around the right corner o and the lower sign refers to rocking around the left corner o' . Either the upper sign or the lower sign can be used for full contact phase.

In Figures 5–7, the free vibration is initiated with a non-zero θ ($0.8\alpha_{cg}$) while the initial $\dot{\theta}$, u and \dot{u} all set to zero. In each figure, the dimensionless rocking angle (θ/α_{cg}), dimensionless elastic translational displacement (u/u_{cr}), dimensionless energy response (E/E_{ref}) and velocity responses are plotted in the corresponding sub-figures (e.g. Figures 5(A)–5(D)). In each sub-figure (e.g. Figure 5(A)), responses obtained with IM1, IM2 and IM3 are shown with red, black and blue lines, respectively. Figure 5(A) shows the time histories of rocking angle obtained according to the three impact models using the structure of Example 1, which represents a stiff structure. Prior to the first impact, the responses of all three models are identical. The three models diverge after the first impact. The inset figures (presenting a zoomed-in view of the behaviour around first impact at around 2.05 s) shows that IM1 and IM2 simulations directly proceed to a new rocking phase while IM3 simulation transits to a full contact phase at this impact. The imposed direct transition to a full contact phase leads to substantial elastic translational displacements following the impact, as shown in Figure 5(B). It is of interest to determine λ_0 required to proceed to a full contact phase at the first impact by evaluating Equation (25). This yields $\lambda_0 = -5.13$, i.e. J_y is applied at a location that is at 5.13 times the half-width of the structure in the direction opposite of the vector pointing from the post-impact rocking corner to the pre-impact one. This negative λ_0 value indicates a mechanically inadmissible location for J_y , outside the base of the structure. Such an impulse would require the interface to experience significant tensile stresses during impact, in contrast to the non-tensile assumption used for the interface. Additionally, this imposed value for λ is substantially different to the commonly employed value of $\lambda = 0$ used in the literature. These observations highlights the need for impact models to consider the possibility for a transition to a rocking phase upon impact, as proposed by IM1 and IM2.

Furthermore, Figure 5(C) shows that IM3 simulations led to an overall larger energy dissipation for this stiff structure. By contrast, IM1 and IM2 models indicate a similar rocking response in Figure 5(A) for a stiff structure, with some intriguing differences. The inset figure in 5(A) highlights that time histories of θ/α_{cg} are different after impact, but they converge to one another after a short duration. The coefficient of restitution at impact was calculated as 0.72 and 0.96,

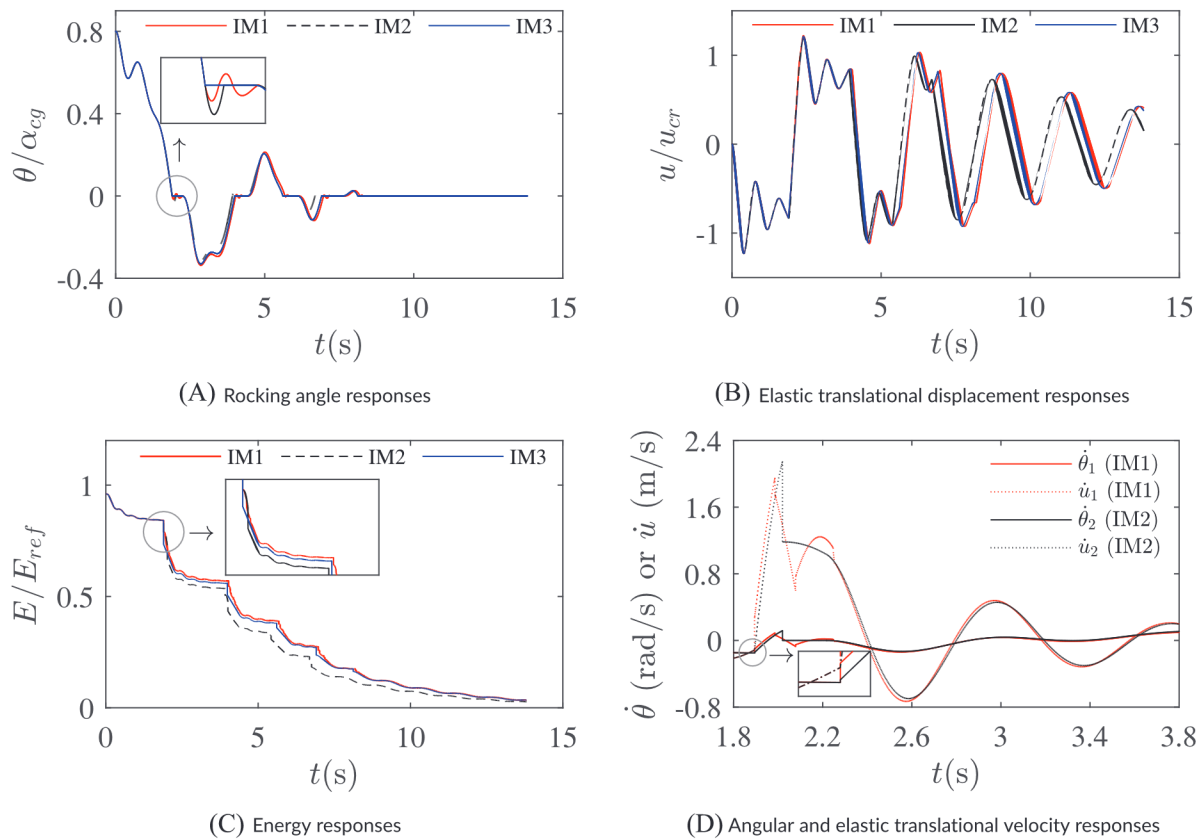


FIGURE 7 Example 3: free vibration responses of a flexible structure ($\omega_n = 2.4313p$)

for IM1 and IM2 simulations, respectively. However, as a result of the energy transfer between the top mass and the ‘U’ structure, and the ensuing energy dissipation due to the damper, the elastic translational velocity \dot{u} of the top mass is effectively transferred back to the $\dot{\theta}$ in the IM1 simulation. This mechanism was described in Section 3 at the limit of the spring being infinitely stiff, however the same qualitative behaviour is observed for an effectively stiff spring. As a result, for this sufficiently stiff FRM, θ/α_{cg} in IM1 and IM2 simulations yield very similar results. Nonetheless, due to the finite stiffness of the oscillator, there are minor differences between the responses predicted by IM1 and IM2 simulations. These are more noticeable in Figure 5(D), which shows $\dot{\theta}$ and \dot{u} responses immediately after the first impact.

After an examination of a stiff structure, it is of interest to explore the trends for more flexible structures, where the three impact models are expected to lead to different results. For the intermediately stiff structure (Example 2) in Figure 6, the kinetic energy stored in elastic translational motion transfers back to the rotational motion after the first impact in a short time for IM1 simulation. The responses for IM1 and IM2 simulations are therefore similar until around 6 s. At around this time, an impact occurs when a transition to rocking is predicted for IM2 simulation while IM1 simulation experiences three consecutive impacts, which leads to divergence between the responses of IM1 simulation and IM2 simulation (see inset Figure in 6(A)). With further impacts, the differences between IM1 simulation and IM2 simulation increase further. IM3 simulation experiences different behaviours from IM1 and IM2 simulations as it always forces full contact transition upon impact.

For the most flexible structure of Example 3 (Figure 7), the responses predicted by IM1 simulation and IM2 simulation diverge significantly from the first impact. Here, IM1 simulation experiences, within a very short duration, five impact events transiting between rocking phases, as shown inset in Figure 7(A). These impacts occur due to the interaction between elastic vibration and rocking motion. As discussed in earlier work,^[35] the significant deformational velocities induced during impact may result in a fast reversal of the rocking motion after impact resulting in subsequent impacts within a short duration. The IM2 model also experiences a motion reversal, but this model transits to a full contact phase shortly after, as shown in the inset figure. According to Figure 7(C), IM2 simulation dissipates the most energy. In contrast, IM3 simulation experiences only a single transition to the full contact phase, and dissipates less energy overall. However, it is important to emphasise that the full contact transition is enforced for each impact for IM3 simulation, which requires

TABLE 3 Nondimensional parameters of the effectively rigid structures for the FRM (IM1-IM3)

	Π_1 (ω_n/p)	Π_2 (ζ_n)	Π_3 (α_{cg})	Π_4 (α_A)	Π_5 (ω/p)	$\Pi_6(A/(g \tan$ ($\alpha_{cg})))$	Π_8 (m_A/m)	$\Pi_9(I_A/$ ($m_A R_A^2$))
Case 1	500	0.05	0.1476	0.2841	[0,13]	[0,30]	0.4746	0.5636
Case 2	500	0.05	0.2500	0.2841	[0,8]	[0,12]	0.4746	0.5636

TABLE 4 Key parameters of the effectively rigid structures for the FRM (IM1-IM3)

	$\alpha(\text{rad})$	α_A	$b(\text{m})$	$m(\text{kg})$	$m_A(\text{kg})$	$I_A(\text{kg}\cdot\text{m}^2)$	ω_n/p	ζ
Case 1	0.1200	0.2841	1.0000	3.3173×10^4	1.5744×10^4	1.1295×10^5	500	0.05
Case 2	0.2365	0.2841	1.7022	3.3173×10^4	1.5744×10^4	3.2723×10^5	500	0.05

TABLE 5 Equivalent simulation parameters of the rigid structures for the IPM

	$\alpha_e(\text{rad})$	$b_e(\text{m})$	$m_e(\text{kg})$	$I_e(\text{kg}\cdot\text{m}^2)$
Case 1	0.1476	1.0000	4.8917×10^4	2.6282×10^6
Case 2	0.2500	1.7022	4.8917×10^4	2.6590×10^6

a specific value of λ_0 each time. The values of λ_0 for all the five impacts (from the first to the fifth impact) are -5.90 , -5.92 , -5.79 , -5.89 , -5.71 , which are all mechanically inadmissible.

Figure 7 confirms the finding in earlier work by Vassiliou et al.^[6] that the IM2 model results in significantly greater energy dissipation for flexible structures due to the ensuing consecutive impacts. The IM3-type models were suggested as a means to resolve this issue, but the above discussion highlights how enforcing a full contact transition at every impact may lead to mechanically inadmissible values for the locus of J_y . The new IM1 model appears to resolve the excessive energy dissipation issue within a consistent impact framework and yields similar response predictions to IM3 models for the examined flexible configurations. As demonstrated earlier, the IM1 models have the additional ability to address stiffer configurations, where IM3 predictions result in unrealistic energy dissipation and vibration at impacts. It is necessary to generalise these promising findings for other geometries and loading conditions; this is attempted in the next section.

4.2 | Response to pulse excitations

The FRM with different geometric and structural parameters is examined in this section with IM1, IM2 and IM3 impact models, subjected to horizontal ground accelerations of the form of single cycle sinusoidal pulses as defined in Equation (31). To explore a range of results in a concise manner, stability diagrams are used. Several different types of structure are explored: stiff (effectively rigid) ones (Case 1, Case 2), flexible ones (Case 3, Case 4), structures with zero bottom mass ($m_A/m = 0$, Case 5, Case 6) and structures with zero bottom mass height ($h_A = 0$, Case 7, Case 8). The properties of these models are summarised in Tables 3–8. Note that λ is set 0 whenever possible and hence is not included for simplicity in all the tables showing simulation parameters.

First, Cases 1 and 2 were used to study the stability of effectively rigid structures (i.e. with large lateral stiffness). Stability diagrams computed using the FRM (with IM1, IM2 and IM3) and the IPM are presented to highlight trends. Two such FRM structures (with centre of gravity slenderness 0.1476 and 0.2500) were chosen as indicated with the dimensionless parameters in Table 3. The following physical parameters were chosen for the structures: $p = 1.1143 \text{ s}^{-1}$, $g = 9.81 \text{ m}\cdot\text{s}^{-2}$, $m = 3.3173 \times 10^4 \text{ kg}$. Other resultant key parameters for the two structures are highlighted in Table 4. To compare the FRM and the IPM, suitable geometries need to be determined for the IPM that are equivalent to the FRM geometry. The two equivalent rocking structures for the IPM are obtained as follows: $p_e = p$, $\alpha_e = \alpha_{cg}$, $m_e = m_A + m$, $I_e = I_A + m_A R_A^2 + m R^2$, where p_e and α_e denote the rocking frequency and slenderness of the IPM structure, respectively. m_e is the mass, while I_e is its mass moment of inertia about the corner. The resultant key parameters for the two equivalent IPM structures are shown in Table 5.

The comparisons between the stability diagrams for single cycle sinusoidal pulses are presented in Figure 8. The horizontal axes in all figures showing stability diagrams in this section denote the dimensionless frequency of the excitations, while the vertical axes denote their dimensionless amplitude. Three areas are highlighted in the stability diagrams: the

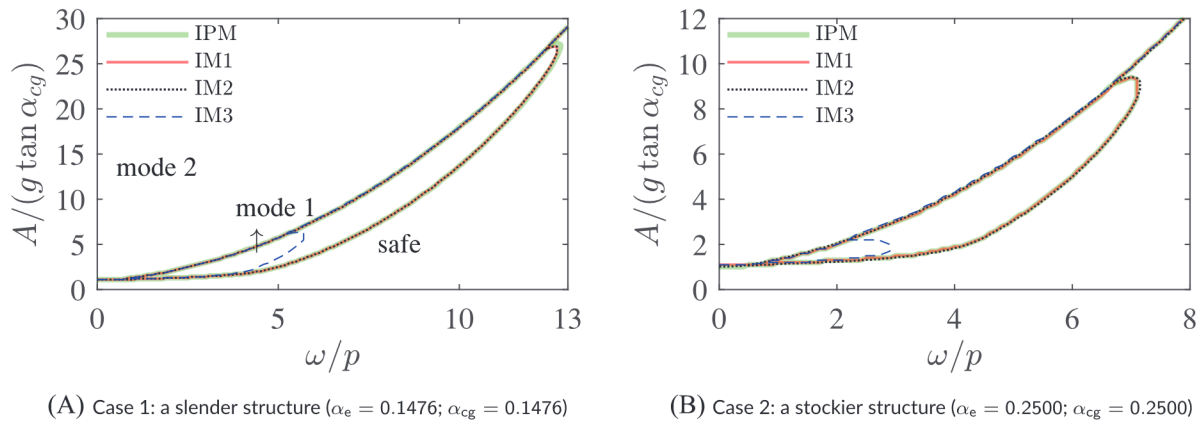


FIGURE 8 Stability diagrams of the effectively rigid cases ($\omega_n/p = 500$)

TABLE 6 Simulation parameters for the flexible cases

	Π_1 (ω_n/p)	Π_2 (ζ_n)	Π_3 (α_{cg})	Π_4 (α_A)	Π_5 (ω/p)	$\Pi_6(A/(g \tan(\alpha_{cg})))$	Π_8 (m_A/m)	$\Pi_9(I_A/(m_A R_A^2))$
Case 3	2.4313	0.05	0.1476	0.2841	[0,6]	[0,6]	0.4746	0.5636
Case 4	2.4313	0.05	0.2500	0.2841	[0,6]	[0,6]	0.4746	0.5636

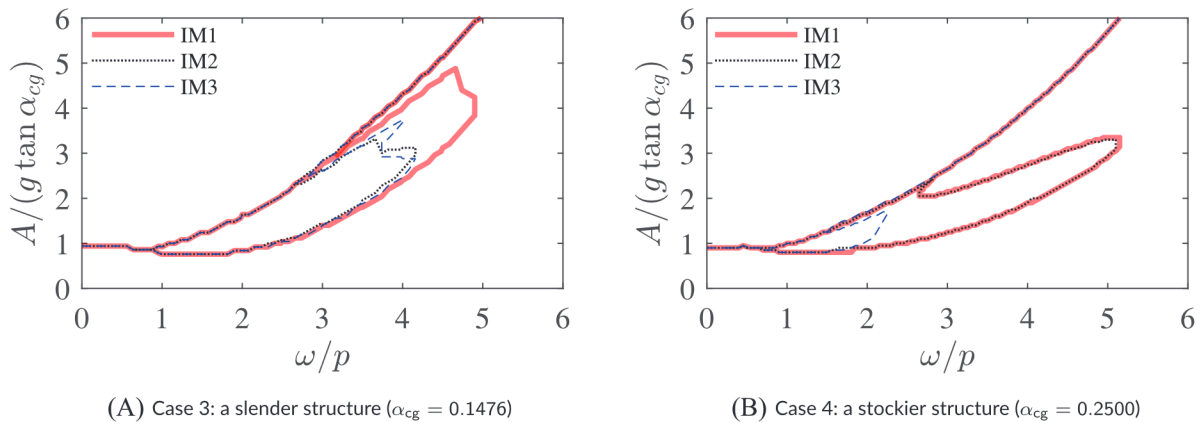


FIGURE 9 Stability diagrams of the flexible cases ($\omega_n/p = 2.4313$)

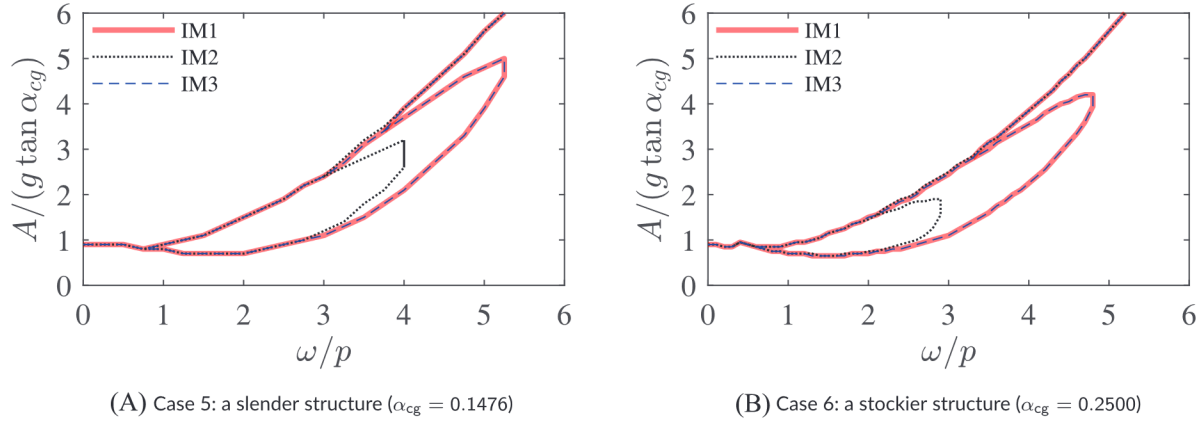
mode 1 collapse area, the mode 2 collapse area and the safe area. These, respectively, correspond to the structure collapsing having previously experienced one or more impacts, the structure collapsing without having previously experienced impacts, and the structure not collapsing. As can be seen in Figure 8(A), the three different areas are annotated by corresponding names. The curves plotted in the figure indicate the boundaries between the three areas for each impact model. The positions of these three areas around the corresponding boundaries are similar throughout the paper, and annotations of these areas are omitted for simplicity in other stability diagrams.

The results obtained from IM1, IM2 and the IPM simulations are almost identical for both Case 1 (Figure 8(A)) and Case 2 (Figure 8(B)). Given the good agreement between the three models, it is reasonable to conclude that the IM1 is consistent with the IPM treatment as lateral stiffness tends to infinity. However, IM3 simulations predict a very small mode 1 collapse area compared with the other three models. This further indicates that IM3 simulations are underestimating failure for laterally stiff structures.

After investigating the effectively rigid structures, Cases 3 and 4 are explored to compare impact models for very flexible structures ($\omega_n/p = 2.4313$, similar to Example 3 in Figure 7). The parameters for these two cases are shown in Table 6, and the resultant stability diagrams are shown in the following Figures 9(A) and 9(B).

TABLE 7 Simulation parameters for the zero bottom mass cases

	Π_1 (ω_n/p)	Π_2 (ζ_n)	Π_3 (α_{cg})	Π_4 (α_A)	Π_5 (ω/p)	$\Pi_6(A/(g \tan(\alpha_{cg})))$	Π_8 (m_A/m)	$\Pi_9(I_A/(m_A R_A^2))$
Case 5	2.4313	0.05	0.1476	0.2841	[0,6]	[0,6]	0	0
Case 6	2.4313	0.05	0.2500	0.2841	[0,6]	[0,6]	0	0

**FIGURE 10** Stability diagrams of the zero bottom mass cases ($m_A/m = 0$)

According to the results of Case 3 and 4 shown in Figure 9, the three impact models influence the stability diagrams in a number of different ways but the trends observed earlier for free vibration motion are still applicable. To start with, it is useful to note that the borders of the area that defines collapsing without impact are the same for IM1, IM2 and IM3 simulations. This is to be expected, since these models only affect behaviour after impact.

The differences among the three models are seen for the mode 1 collapse area and the safe area. IM1 simulations predict a larger collapse region due to mode 1. The other two models underestimate the collapse region. For IM2 simulations, this is a consequence of the spring and damper transmitting impulses during impact, while in IM3 simulations that is a result of always enforcing a post-impact transition to full contact. This finding is in accordance with the earlier observation that both IM2 and IM3 simulations can overestimate energy dissipation.

Figure 9(B) demonstrates the stability diagram of a less slender but equally flexible structure than the one studied in Figure 9(A). Here IM3 simulations indicate a notably small mode 1 collapse area, while IM2 simulations appear to be in agreement with IM1 simulations. This can be explained by the tendency of IM3 simulations to dissipate more significant energy for less slender structures, by enforcing the structure to a full contact phase upon impact.

Flexible structures with a single lumped mass at the top and no bottom mass have been investigated by previous studies.^[3–5,7] This special scenario is examined using the FRM by setting the mass ratio to zero (i.e. $m_A/m = 0$), which includes two cases in Table 7: Cases 5 and 6. Two structures with different slenderness are considered for these cases, $\alpha_{cg} = 0.1476$ and $\alpha_{cg} = 0.2500$, respectively. The associated stability diagrams are shown in the following Figure 10.

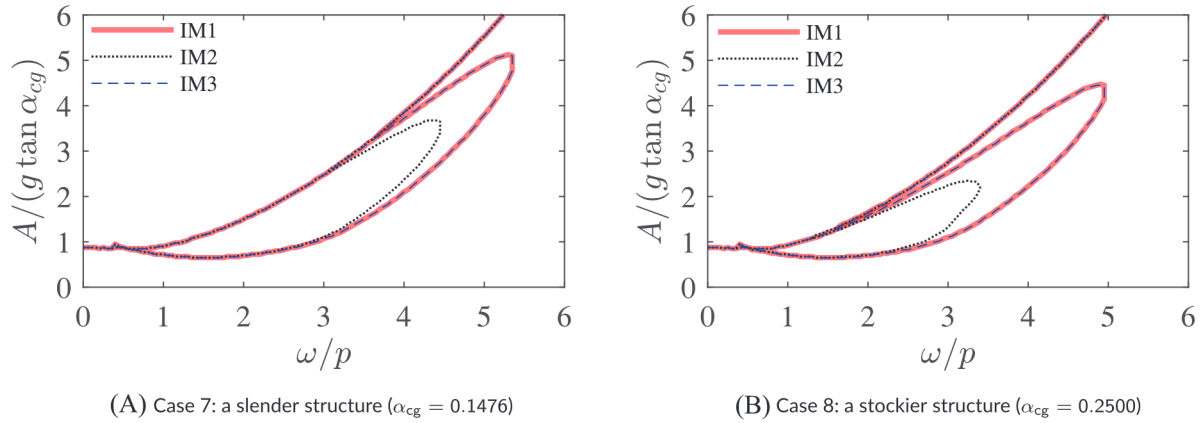
In Figure 10, it can be seen that the results of IM3 simulations converge to those of IM1 simulations, however, by contrast, IM2 simulations underestimate mode 1 collapse areas when compared to IM1 simulations. The similar behaviours of IM1 and IM3 simulations can be investigated through an examination of the coefficient of restitution for IM1. For this zero bottom mass case ($m_A/m = 0$), the corresponding coefficient of restitution for IM1 can be obtained by substituting $m_A = 0$, $I_A = 0$ and $\lambda = 0$ into Equation (19), which results in the following equation:

$$e = \frac{u^2 - b^2}{(u \pm b)^2} \quad (46)$$

It can be concluded from Equation (46) that $e > 0$ only if $|u| > b$. As it is unlikely that the elastic translational displacement becomes larger in magnitude than the half-width b for a reasonable designed system and excitations of practical magnitude, the previous condition practically almost always leads to a negative value of e . Consequently IM1 simulations would have selected full contact as the post impact phase for any impact. For such cases, IM1 simulations will converge to IM3 simulations, as long as $|u| \leq b$. Under this condition, evaluating Equation (25) yields $\lambda_0 = 1 \pm u/b$, which indi-

TABLE 8 Simulation parameters for the zero bottom mass height cases

	Π_1 (ω_n/p)	Π_2 (ζ_n)	Π_3 (α_{cg})	Π_4 (α_A)	Π_5 (ω/p)	$\Pi_6(A/(g \tan(\alpha_{cg})))$	Π_8 (m_A/m)	$\Pi_9(I_A/(m_A R_A^2))$
Case 7	2.4313	0.05	0.1476	$\pi/2$	[0,6]	[0,6]	0.4746	0.5636
Case 8	2.4313	0.05	0.2500	$\pi/2$	[0,6]	[0,6]	0.4746	0.5636

**FIGURE 11** Stability diagrams of the zero bottom mass height cases ($h_A = 0$)

cates λ_0 takes values between 0 and 2 for IM1 simulations. Therefore λ_0 is always mechanically admissible under these circumstances ($m_A/m = 0$, and $|u| < b$), and IM1 can systematically determine the need to transit to full contact.

Similarly, a number of studies considered rocking structures with the bottom mass located at zero height ($h_A = 0$).^[6] This special scenario is also considered with the parameters shown in Table 8. Again, two cases with different slenderness of centre of gravity are chosen, Case 7: $\alpha_{cg} = 0.1476$ and Case 8: $\alpha_{cg} = 0.2500$. The stability diagrams are shown in Figure 11.

Yet again, it can be seen that the stability diagrams of IM3 simulations converge to those of IM1 simulations for both Cases 7 and 8. In order to find the reason for this, the coefficient of restitution with a zero bottom mass height for IM1 simulations is analysed. Substituting $h_A = 0$ and $\lambda = 0$ into Equation (19), the corresponding coefficient of restitution can be obtained as Equation (47).

$$e = \frac{m_A b^2 \left[\Pi_9 - 1 + \frac{1}{\Pi_8 b^2} (u^2 - b^2) \right]}{I_A + m_A b^2 + m(u \pm b)^2} \quad (47)$$

The sign of the coefficient of restitution is the same as the sign of $\Pi_9 - 1 + \frac{1}{\Pi_8 b^2} (u^2 - b^2)$. $\Pi_9 - 1$ is always negative since $I_A/(m_A R_A^2)$ is always smaller than 1 for geometries of practical interest. Thus, e would be negative when $|u| < b$ before impact. In that case, the IM1 model would reject rocking as a post-impact phase and instead select full contact, a choice that is always enforced in IM3 simulations. Therefore, IM1 and IM3 simulations would be equivalent if the structure with its bottom mass at zero height is reasonably stiff to the extent that for the applied excitations $|u| < b$.

It is important to emphasise that the consideration of a zero bottom mass or a zero bottom mass height is a special scenario, with limited practical applications. However, the new impact model IM1 is able to consistently treat these special scenarios (Cases 5–8) as well as the more general cases of bottom mass geometry (Cases 3 and 4) within the same unified framework, while ensuring agreement with established impact models, such as the IPM, for cases where the structure can practically be considered as rigid (Cases 1 and 2).

5 | CONCLUSIONS

This paper revisits the existing formulations for laterally flexible rocking oscillators. To enable the consideration of a wider array of geometrical configurations, previous flexible rocking oscillator models were updated to include the height and

mass moment of inertia of the bottom mass. Equations of motion were then derived for each phase of motion (i.e. full contact and rocking phases).

A review highlighted the divergent assumptions concerning the treatment of impact in previous models. To address the shortcomings of these models, a new impact model is developed. This impact model is based on the principle that the spring and damper components of the flexible rocking oscillator cannot transfer horizontal impulses during infinitesimally small duration impacts. When this principle is combined with the consideration of a variable impulse locus under the structure, a series of momentum conservation equations emerge, which are consistently used to determine the post-impact parameters. The model is completed by a criterion for deciding whether the next phase of motion will be a full contact or a rocking phase. Analytical derivations demonstrate that the new impact model yields equivalent results to Housner's IPM model at the limit of the spring becoming practically rigid. The result was demonstrated to hold in examples for sufficiently stiff springs. Through free vibration time history simulations and stability diagrams under pulse excitations for a range of structures, it was shown that the new impact models are broadly applicable to structures with different flexibilities. The new models do not suffer from excessive energy dissipation issues and unify the divergent assumptions from previous research in a consistent modelling framework.

ACKNOWLEDGEMENT

The first author would like to thank China Oxford Scholarship Fund for supporting his research financially.

DATA AVAILABILITY STATEMENT

Research data are not shared.

ORCID

Huanian Zhu  <https://orcid.org/0000-0002-2799-6915>

Manolis N. Chatzis  <https://orcid.org/0000-0002-0917-8134>

Sinan Acikgoz  <https://orcid.org/0000-0002-3901-574X>

REFERENCES

1. Housner GW. The behavior of inverted pendulum structures during earthquakes. *Bull Seismol Soc Am*. 1963;53(2):403–417.
2. Makris N, Aghagholizadeh M. Effect of supplemental hysteretic and viscous damping on rocking response of free-standing columns. *J Eng Mech*. 2019;145(5):04019028.
3. Acikgoz S, DeJong MJ. The interaction of elasticity and rocking in flexible structures allowed to uplift. *Earthq Eng Struct Dyn*. 2012;41(15):2177–2194.
4. Meek JW. Effects of foundation tipping on dynamic response. *J Struct Div*. 1975;101(7):1297–1311.
5. Chopra AK, Yim SCS. Simplified earthquake analysis of structures with foundation uplift. *J Struct Eng*. 1985;111(4):906–930.
6. Vassiliou MF, Truniger R, Stojadinović B. An analytical model of a deformable cantilever structure rocking on a rigid surface: development and verification. *Earthq Eng Struct Dyn*. 2015;44(15):2775–2794.
7. Oliveto G, Calio I, Greco A. Large displacement behaviour of a structural model with foundation uplift under impulsive and earthquake excitations. *Earthq Eng Struct Dyn*. 2003;32(3):369–393.
8. Acikgoz S, DeJong MJ. Analytical modelling of multi-mass flexible rocking structures. *Earthq Eng Struct Dyn*. 2016;45(13):2103–2122.
9. Cappelli E, Di Egidio A, Vestroni F. Analytical and experimental investigation of the behavior of a rocking masonry tuff wall. *J Eng Mech*. 2020;146(6):04020048.
10. Kalliontzis D, Schultz AE, Sritharan S. Generalized dynamic analysis of structural single rocking walls (SRWs). *Earthq Eng Struct Dyn*. 2020;49(7):633–656.
11. Di Egidio A, Leo dAM, Simoneschi G. Effectiveness of mass–damper dynamic absorber on rocking block under one-sine pulse ground motion. *Int J Non Linear Mech*. 2018;98:154–162.
12. Chatzis M, Espinosa MG, Smyth A. Examining the energy loss in the inverted pendulum model for rocking bodies. *J Eng Mech*. 2017;143(5):04017013.
13. Zhu H, Chatzis M, Acikgoz S. The influence of impact modelling assumptions on the dynamic behaviour of flexible rocking oscillators. In: *Proceedings of the COMPDYN*. 2021.
14. ElGawady MA, Ma Q, Butterworth JW, Ingham J. Effects of interface material on the performance of free rocking blocks. *Earthq Eng Struct Dyn*. 2011;40(4):375–392.
15. Psycharis IN, Jennings PC. Rocking of slender rigid bodies allowed to uplift. *Earthq Eng Struct Dyn*. 1983;11(1):57–76.
16. Koh AS, Spanos PD, Roesset JM. Harmonic rocking of rigid block on flexible foundation. *J Eng Mech*. 1986;112(11):1165–1180.
17. Yuan L. *The Effect of Foundation Flexibility on the Dynamic Response of a Rigid Block*. University of Notre Dame; 2006.
18. Palmeri A, Makris N. Response analysis of rigid structures rocking on viscoelastic foundation. *Earthq Eng Struct Dyn*. 2008;37(7):1039–1063.
19. Chatzis M, Smyth A. Robust modeling of the rocking problem. *J Eng Mech*. 2012;138(3):247–262.



20. Psycharis IN. Dynamics of flexible systems with partial lift-off. *Earthq Eng Struct Dyn*. 1983;11(4):501–521.
21. Psycharis IN. Effect of base uplift on dynamic response of SDOF structures. *J Struct Eng*. 1991;117(3):733–754.
22. Ishiyama Y. Motions of rigid bodies and criteria for overturning by earthquake excitations. *Earthq Eng Struct Dyn*. 1982;10(5):635–650.
23. Sinopoli A. Dynamics and impact in a system with unilateral constraints the relevance of dry friction. *Meccanica*. 1987;22(4):210–215.
24. Shenton III HW, Jones NP. Base excitation of rigid bodies. I: Formulation. *J Eng Mech*. 1991;117(10):2286–2306.
25. Lipscombe P, Pellegrino S. Free rocking of prismatic blocks. *J Eng Mech*. 1993;119(7):1387–1410.
26. Chatzis M, Smyth A. Modeling of the 3D rocking problem. *Int J Non Linear Mech*. 2012;47(4):85–98.
27. Zulli D, Contento A, Di Egidio A. 3D model of rigid block with a rectangular base subject to pulse-type excitation. *Int J Non Linear Mech*. 2012;47(6):679–687.
28. Spanos PD, Roussis PC, Politis NP. Dynamic analysis of stacked rigid blocks. *Soil Dyn Earthq Eng*. 2001;21(7):559–578.
29. Chatzis M, García Espinosa M, Needham C, Williams M. Energy loss in systems of stacked rocking bodies. *J Eng Mech*. 2018;144(7):04018044.
30. Makris N, Black CJ. Dimensional analysis of rigid-plastic and elastoplastic structures under pulse-type excitations. *J Eng Mech*. 2004;130(9):1006–1018.
31. Buckingham E. On physically similar systems; illustrations of the use of dimensional equations. *Phys Rev*. 1914;4(4):345–376.
32. Shampine LF, Reichelt MW. The MATLAB ODE suite. *SIAM J Sci Comput*. 1997;18(1):1–22.
33. Zhang J, Makris N. Rocking response of free-standing blocks under cycloidal pulses. *J Eng Mech*. 2001;127(5):473–483.
34. Acikgoz S, DeJong MJ. The rocking response of large flexible structures to earthquakes. *Bull Earthq Eng*. 2014;12(2):875–908.
35. Acikgoz S, DeJong MJ. A simple model to quantify rocking isolation. *Bull N Z Soc Earthq Eng*. 2018;51(1):12–22.

How to cite this article: Zhu H, Chatzis MN, Acikgoz S. A new impact model for the flexible rocking oscillator. *Earthquake Engng Struct Dyn*. 2022;51:1819–1839. <https://doi.org/10.1002/eqe.3639>

